Lomakin, Ivan; Nigmatullina, Alfiia; Sauvage, Xavier

Nanostructuring of beryllium bronze : Contribution of grain boundaries segregation and solid solution

Nanostructuring of beryllium bronze: Contribution of grain boundaries segregation and solid solution

Ivan Lomakin [a,*], Alfiia Nigmatullina [b], Xavier Sauvage [c]

[a] Aalto University, Department of Applied Physics, Complex Systems and Materials Group, P.O. Box 11100, 00076 Aalto, Espoo, Finland
[b] Saint Petersburg University, Laboratory For Mechanics of Bulk Nanostructured Materials, Saint Petersburg 198504, Russia
[c] Univ Rouen Normandie, INSA Rouen Normandie, CNRS, Groupe de Physique des Matériaux, UMR6634, 76000 Rouen, France

A R T I C L E   I N F O

A B S T R A C T

The impact of composition on grain refinement in solutionized Cu-Be alloys was investigated. High-pressure torsion resulted in grain sizes of 10–110 nm for Cu–1 wt.% Be and 10–20 nm for Cu-2 wt.%Be. Our findings indicate that Be stabilizes the nanoscale grain size, which is influenced by the balance between defect creation and annihilation. Consequently, Be concentration serves as a key parameter for directing microstructure and property changes during severe plastic deformation.

1. Introduction

Addition of alloying elements to pure metals accompanied by cold working is efficient method to tune the desired properties of materials. As an example of the extreme state that can be achieved, severe plastic deformation (SPD) may produce ultrafine grain (UFG) structures [1]. Initial chemical composition, even impurities in a small amount, may significantly affect [2] final structure and, thus, properties. Solute elements affect both the mobility and the stability of crystalline defects and various mechanisms might be involved during SPD, such as delayed recovery of dislocation [3], reduced boundary mobility [4] and segregations [5]. To shed a light on these mechanisms the influence of Be concentration in solubilized Cu–Be alloys was investigated. This system was selected since it is among alloys exhibiting the strongest grain refinement by SPD [6,7].

2. Methods

To obtain two different compositions, a Cu-2 wt.% Be master alloy was mechanically mixed with pure Cu using High Pressure Torsion (HPT) of two sectors (total diameter of 20 mm) combined together (Fig.1a. The sector of Cu-2 wt.% Be master alloy was solutionized at 780°C for 2 h before HPT processing with Cu at 400°C up to 100 revolutions under 6 GPa at 1 rpm using a Walter Klement GmbH press equipped with an induction heating device.

Afterward, a coarse-grained and homogenized Cu-1 wt.% Be alloy

was obtained by annealing at 850°C for 5 h. Subsequently, both this alloy and the master Cu-2 wt.% Be alloy were solutionized and processed by HPT at room temperature for 10 revolutions (6 GPa, 1 rpm) to achieve UFG structures. Homogeneity and properties were assessed through micro-hardness measurements conducted with a Shimadzu-G21DT testing machine, applying a 0.5 kg load. Structures were characterized by X-ray diffraction analyses using a Brucker D8 Discover diffractometer (CuKα radiation, 5°/min) and transition electron microscopy (TEM) with a JEOL ARM-200F microscope operated at 200 kV in scanning mode. High angle annular dark field (HAADF) and dark field (DF) images were recorded with collection angles of 80–180 mrad and 20 – 80 mrad respectively. Thermal stability was assessed with Differential Scanning Calorimetry (DSC) using a NETZSCH DSC 204 F1 Phoenix calorimeter. 10 mg specimens underwent two thermal cycles from 20°C to 550°C at a heating and cooling rate of 5°C/min. The provided curves were obtained by subtracting data from the first cycle and the second cycle performed under similar conditions.

3. Results

To examine the homogeneity of the mechanically mixed Cu - 1 wt.% Be alloy achieved by HPT sector processing, a microhardness map was measured in the cross section after annealing and subsequent HPT (Fig. 1b). This map exhibits hardness fluctuations ranging from 315 to 380 HV indicating a relatively homogeneous material with a mean hardness value (350 HV) lower than that of the Cu-2 wt.% Be alloy

---

processed in similar conditions (390 HV) [7].

STEM-HAADF images (Figs. 2a and 2b) clearly show that the mean grain size is in the sub-micron range for both alloys and that significant Be segregation occurred along grain boundaries (GBs) during SPD (dark contrast at GBs). This contrast was used to measure the grain size [6]. However, the mean grain size is significantly larger in the Cu-1 wt.%Be alloy (61 nm) than in Cu-2 wt.%Be alloy (20 nm) and the grain size distribution is also wider (Fig. 2c). Thus, grain refinement mechanisms are similar in both alloys but the amount of Be in solid solution directly influences the final grain size achieved by SPD.

The Be content minimally affects the fcc Cu lattice parameter. X-ray diffraction shows a slight shift in the Cu(111) and (022) peaks for Cu-1 wt. Be and Cu-2 wt. Be alloys, both after homogenization and SPD processing (Fig. 3), indicating most Be is in solid solution in the UFG state. Interplanar spacing decreases due to lower Be concentration and its interstitial nature as a copper alloying element [8]. Significant peak broadening is mainly due to grain size reduction and internal stresses, more pronounced in Cu-2 wt.%Be alloy, consistent with TEM observations (Fig. 2).

The Cu-Be binary system goes through multiple phase transitions during heating, progressing from Guinnier-Preston (GP) zones to the γ stable phase [6], as observed in the DSC curve for coarse-grained Cu-2 wt.% Be (Fig. 4a). For lower Be content, phase kinetics involve an incomplete transition ending with γ'' (peak B), followed by complete precipitate dissolution and the formation of α–supersaturated solid solution through an endothermic phase transition (peak D) (Fig. 4a) [9,10]. The shift to lower temperatures and reduced heat release is driven by a higher transition driving force due to lower internal stresses and reduced intermetallic phase fraction. These transitions overlap with recovery and recrystallization processes in the SPD state, the Cu-2 wt.% Be alloy storing more energy due to its smaller grain size (Fig. 2) and higher equilibrium intermetallic phase fraction.

4. Discussion

Experimental data shows that the Be content in solid solution greatly impacts the final grain size after SPD, with notable GB segregation observed in all cases by TEM. For each grain, the total amount of beryllium n_{Be}^{total} is the sum of atoms located in the matrix n_{Be}^{mat} and half of those located at GBs (since it is shared with the neighboring grain) n_{Be}^{gb}:

$$n_{Be}^{total} = n_{Be}^{mat} + \frac{n_{Be}^{gb}}{2} \tag{1}$$

Assuming that grains are spherical with a diameter d, the number of atomic sites on the fcc lattice inside the grain N^{mat} and at the boundary N^{gb} can be estimated as follow:

$$N^{mat} = \frac{\pi d^3}{6a_{Cu}^3} \tag{2}$$

$$N^{gb} = \frac{2\pi d^2}{a_{Cu}^2} \tag{3}$$

where a_{Cu} is fcc matrix lattice parameter. Then, assuming that GBs are covered with monolayer of Be, Eq. (1)–(3) lead to:

$$X_{Be}^0 = X_{Be}^{mat} + \frac{3a_{Cu}}{2d} \tag{4}$$

where X_{Be}^0 is the mole fraction of Be in the alloy ($X_{Be}^0 = n_{Be}^{total}/N^{mat}$) and X_{Be}^{mat} is the mole fraction of Be in solid solution inside the grain ($X_{Be}^{mat} = n_{Be}^{mat}/N^{mat}$). From Eq. 4, a nominal composition of 2 wt.% or 12 at.% (or 1 wt.% or 6 at.%) with a mean grain size of 20 nm (or 61 nm) results in approximately 10 at.% (or 5 at.%) of Be in solid solution. These calculations align with XRD data (Fig. 3), which indicates no significant peak shift after HPT for both alloys and a difference in lattice parameters for the 1% and 2% alloys before and after HPT.

Grain boundary segregation in the Cu-Be system reduces grain boundary energy and mobility, promoting ultrafine grain (UFG) structures. While some Be atoms segregate along grain boundaries, most remain in solid solution. This segregation has a composition different from that in the matrix [11] and stabilizes nanoscale grain sizes, resulting in much finer structures compared to commercially pure Cu processed by SPD. After SPD, the Cu-2 wt.%Be alloy exhibits a significantly smaller grain size (20 nm vs. 61 nm in Cu-1 wt.%Be). The grain size depends on the balance between defect creation and annihilation during continuous dynamic recrystallization, as seen in the CuSn system
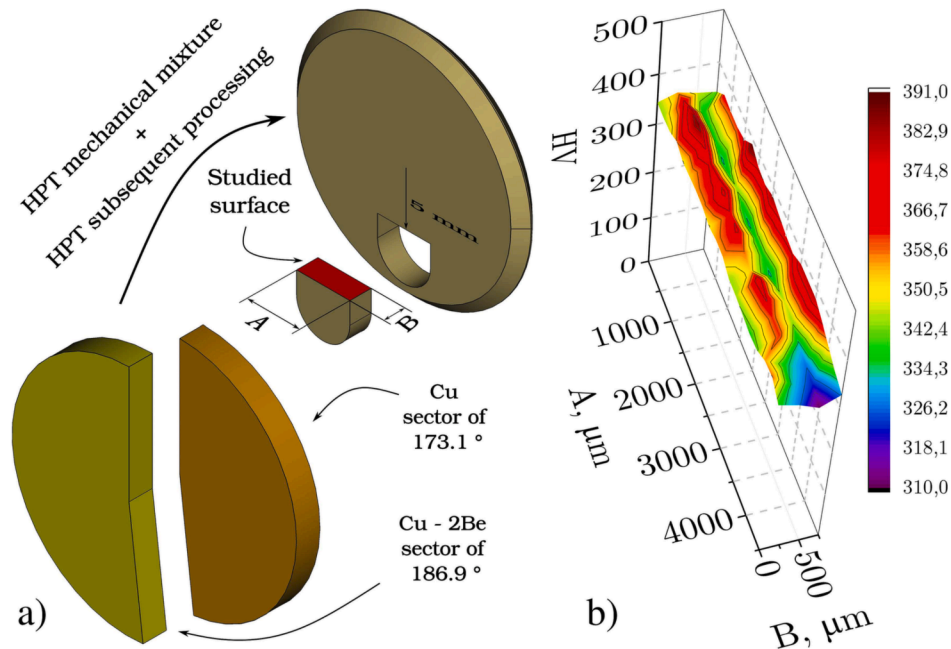

Fig. 1. Schematic representation of the sectors used for HPT and location of the HV map (a). Microhardness of Cu – 1 wt.% Be alloy after HPT sector processing, homogenization and subsequent room temperature HPT processing (b).
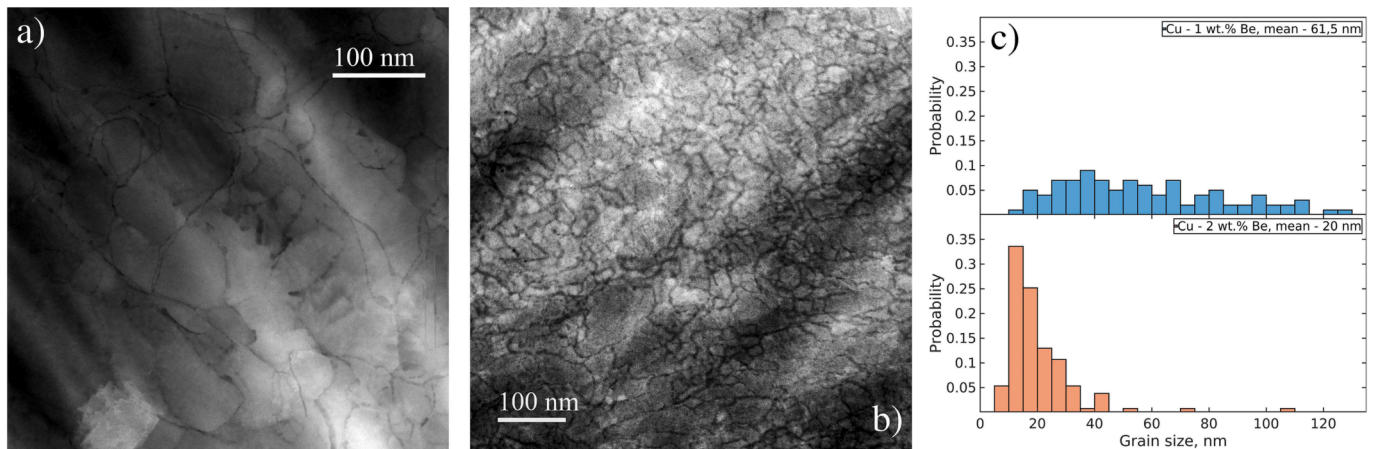
Fig. 2. STEM HAADF images of the Cu-1 wt.%Be (a) and Cu-2 wt.%Be (b) alloys, subjected to severe plastic deformation. (c) - grain size distribution histogram in as-processed Cu-1 wt.%Be and Cu-2 wt.%Be [6].
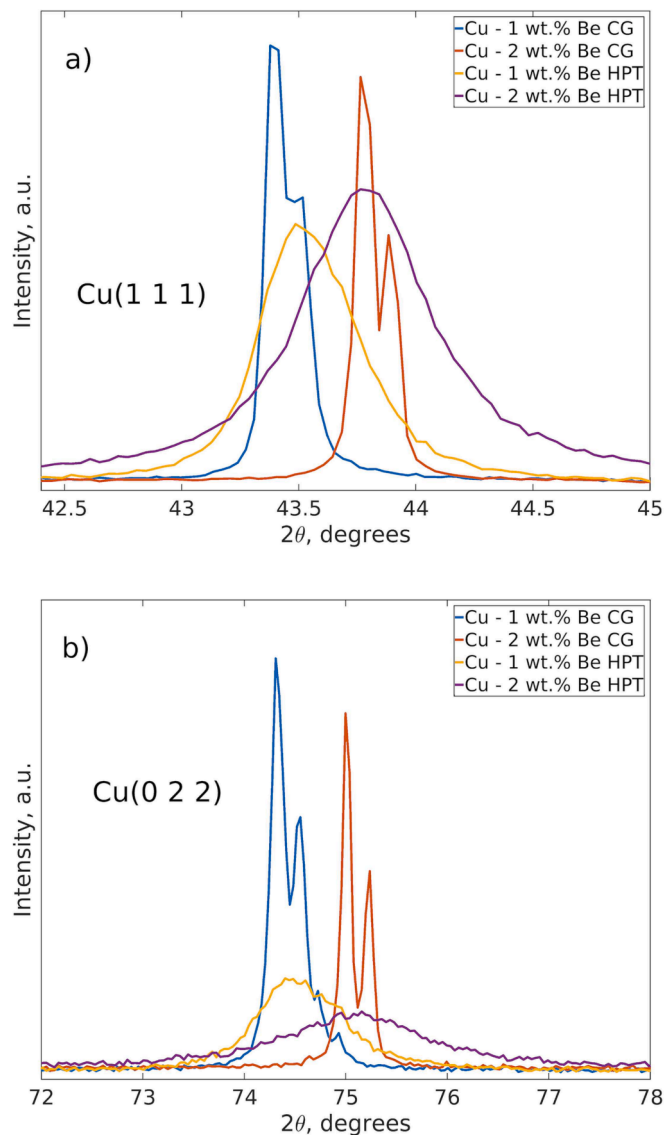

Fig. 3. XRD patterns showing the influence of Be concentration and severe plastic deformation processing on (1 1 1) (a) and (0 0 2) (b) copper matrix peaks for Cu–1 wt.%Be nominal composition) and Cu-2 wt.%Be alloys.

[12]. A higher Be content in solid solution likely reduces dislocation mobility with associated recovery processes, enhancing stability with grain size reduction through GB segregations [12]. This correlates well with the observation that despite inhomogemenius Be atoms redistribution and nonuniformed final grain size for Cu-1 wt.%Be, copper XRD peak have the same width as for homogeneous Cu-2 wt.%Be, i.e. local composition variation still leads to similar solid solution Be concentration in the matrix, only affecting a final grain after processing which is defined by local composition during recrystallization.

5. Conclusions

Mixing copper and Cu-2 wt.%Be alloy through HPT at high temperature, followed by homogenization, creates non-uniform Be atom redistribution, causing variations in composition. This leads to a wide range of final grain sizes after subsequent HPT processing.

Further studies revealed that continuous recrystallization forms new grain boundaries, with the final grain size determined by balance between defect creation and annihilation. Beryllium segregation stabilizes grain size after unloading, particularly in high-beryllium compositions, by reducing dislocation mobility. In the Cu-Be system, Be concentration can serve as a key factor for tailored microstructure and property changes during severe plastic deformation. Increasing beryllium concentration may even achieve finer grain structures, potentially leading to amorphization.

CRediT authorship contribution statement

Ivan Lomakin: Conceptualization, Formal analysis, Methodology, Investigation, Visualization, Data curation, Writing - original draft, Writing - review & editing. **Alfiia Nigmatullina:** Investigation, Validation, Writing - review & editing. **Xavier Sauvage:** Conceptualization, Formal analysis, Methodology, Investigation, Writing - review & editing.

Declaration of Competing Interest

The authors declare the following financial interests/personal relationships which may be considered as potential competing interests: Ivan Lomakin reports financial support was provided by Academy of Finland. Xavier Sauvage reports financial support was provided by National Centre for Scientific Research. If there are other authors, they declare that they have no known competing financial interests or personal relationships that could have appeared to influence the work reported in this paper.
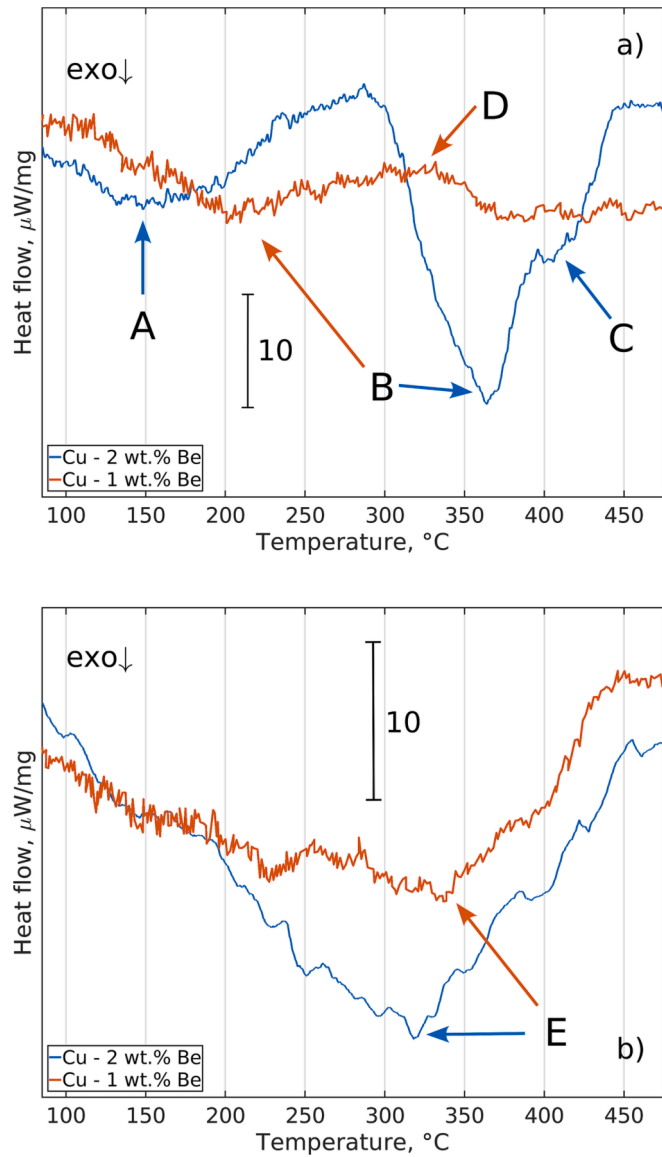
Fig. 4. (a) - DSC curves of Cu-2 wt.%Be and Cu–1 wt.% Be in CG state (b) - DSC curves of Cu-2 wt.%Be and Cu–1 wt.%Be subjected to severe plastic deformation. Peak A - Guinnier-Preston (GP) zones $\to \gamma''$, peak B - $\gamma'' \to \gamma'$, peak C - $\gamma' \to \gamma$, D - $(\gamma + \alpha) \to \alpha$ and peak E - Guinnier-Preston (GP) zones $\to \gamma$ discontinuous precipitation.

References

[1] Kaveh Edalati, et al., Mater. Res. Lett. 10 (4) (2022) 163–256.
[2] R. Tejedor, et al., Mater. Sci. Eng.: A 743 (2019) 597–605.
[3] Yang Liu, et al., Scripta Mater. 159 (2019) 137–141.
[4] Maowen Liu, et al., Materialia 8 (2019), 100448.
[5] Y. Ivanisenko, et al., Adv. Eng. Mater. 20 (10) (2018) 1800443.
[6] I. Lomakin, et al., Mater. Sci. Eng.: A 744 (2019) 206–214.
[7] I. Lomakin, et al., Mater .Sci. Eng.: A 823 (2021), 141760.
[8] A. Almazouzi, et al., Physica Status Solidi (A) 133 (2) (1992) 305–315.
[9] D.J. Chakrabarti, et al., Bull. Alloy Phase Diagrams 8 (3) (1987) 269–282.
[10] D.E. Laughlin, et al., Bull. Alloy Phase Diagrams 2 (1) (1981) 28.
[11] A.A. Mazilkin, et al., Scripta Mater. 173 (2019) 46–50.
[12] Ghenwa Zaher, et al., Materials Today Commun. 26 (2021), 101746.

Data availability

Data will be made available on request.